Bulletin of Engineering Geology and the Environment (2025) 84:105
https://doi.org/10.1007/s10064-025-04133-1

ORIGINAL PAPER

Exploring the deformation characteristics of a steep overhanging anti-dip slope from material mechanics viewpoints

Wen-Chao Huang[1] · Yu-Yi Chang[2] · Wen-Jeng Huang[3] · Jia-Hao Hu[1] · Po-Yen Chao[1]

Received: 11 September 2024 / Accepted: 21 January 2025

Abstract

In this study, we investigated the deformation features of steep overhanging anti-dip slopes based on their scale, the rock layer thickness, and the unsupported length. Centrifuge tests were performed for various configurations of simplified overhanging anti-dip slopes. The steep overhanging anti-dip slopes expressed flexural and block toppling behavior in all of the centrifuge tests in this study. The toppling is a progressive behavior: firstly, the shallow rock layers deform slightly as the deformation starts. Afterward, the deformed rock layers toppled, and the rock layers behind them deformed insignificantly. In terms of the scale effect, increasing the slope scale could raise the toppled and deformed zone of the overhanging anti-dip slope. As the unsupported length of the slope is long, the deformation behavior tends to be flexural toppling. When the rock layer thickness increases, the deformation behavior is similar to block or block-flexure toppling. A normalized bending stiffness (K') is then proposed in this study to discuss the deformation behaviors from material mechanics viewpoints. We found that the K' is related to the toppling behavior of the overhanging anti-dip slopes. With a small K' value, the rock layers in an overhanging anti-dip slope deformed close to a flexural toppling. A much smaller K' value was also obtained for an actual flexural toppling case. Therefore, the findings indicated that the deformability of an overhanging anti-dip slope could be analyzed from a material mechanics viewpoint, and the deformation characteristics depend highly on its normalized bending stiffness.

Keywords Overhanging anti-dip slopes · Centrifuge modeling · Toppling failure · Normalized bending stiffness

Introduction

For the past several decades, the disasters caused by rock slope sliding have resulted in the loss of numerous lives and properties, especially for the residents in the affected areas. Among most rock slope failures, the failure caused by dip slopes is the most disastrous, such as the events in Lincoln Residential Community, Tsaoling landslide, and Formosa Highway in Taiwan. Although the slide-triggering factors are different (rainfall, earthquakes, or gravitational deformation), the sliding scale is sometimes massive, resulting in a vast volume of debris accumulation around the toe area. Due to its scale of failure, the research on dip slopes has been popular for decades, and the failure mechanisms are well-understood. It was found that the dip slope failures are related to the orientations of the planes, the mechanical properties of the geological formations, and the triggering factors. (Tang et al. 2013; Weng et al. 2015; Deng et al. 2017; Lo et al. 2014; Huang et al. 2019). However, the failure of other types of rock slopes, such as anti-dip slopes, may also be related to factors similar to those mentioned above. Based on recent reports of anti-dip slope failure (Lo 2017; Lin et al. 2019), if severe deformation occurs in the anti-dip slope, a failure plane may also be formed and cause large sliding. In the above studies, Lo (2017) studied the typical anti-dip slope failure associated with long-term gravity-induced flexural toppling and Lin et al. (2019) studied the failure mechanism of a steep anti-dip slope from a case study.

In this study, we explored the deformation characteristics of steep overhanging anti-dip slopes with various geometrical parameters and simulated the failure patterns of overhanging anti-dip slopes with realistic scales. Site

✉ Wen-Chao Huang
wenchaoh@g.ncu.edu.tw

[1] Department of Civil Engineering, National Central University, No. 300, Zhongda Rd, 320 Taoyuan, Taiwan

[2] Sinotech Engineering Consultants, Ltd, Taipei, Taiwan

[3] Graduate Institute of Applied Geology, National Central University, No. 300, Zhongda Rd, 320 Taoyuan, Taiwan

Published online: 01 February 2025

investigation and physical tests were adopted as the research approaches in the current study. First, the deformation and failure conditions of a steep overhanging anti-dip slope during a site investigation were summarized. Based on the site investigation results and the deformation features in the literature, several simplified overhanging anti-dip slope models were formulated in physical models to consider influences of the scale effect and geometrical properties on the overhanging slopes. The deformation process and failure patterns were analyzed and discussed under various geometrical features from material mechanics viewpoints. With the proposed non-dimensional normalized bending stiffness and the centrifuge test results, the deformation features observed in the site investigation were also discussed and concluded, hoping to give insights into the deformation features of overhanging anti-dip slopes before the more significant landslide events occur.

Literature reviews

Overhanging anti-dip slope deformation patterns

Müller (1968) was the first to propose the overturning mechanisms of rock columns and blocks for anti-dip slopes with a steep angle. Afterward, Ashby (1971) defined the overturning mechanism as toppling behavior. Cundall (1971) used numerical models to study the toppling behavior with fixed and movable blocks. When the fixed blocks close to the slope face were removed, the blocks behind them moved forward due to the overturning moments of their weights.

Goodman and Bray (1976) and Goodman (1989) classified the three possible main toppling behaviors from field investigation results for anti-dip slopes: block toppling, flexural toppling, and block-flexure toppling. The block toppling could occur for the rock slopes with two sets of orthogonal joints. One of the joint sets is a steep set, of which the spacing usually defines the thickness of the rock layers. The rock columns or blocks are overturned by their weight or pushed by the rock columns behind them. Flexural toppling could occur when there is one major joint set, while the other is not as dominant as the major one. The rock layers tend to bend forward, and tension cracks can be observed in some rock layers. Block-flexure toppling is the combination of the above failure patterns. The tension cracks are fewer than the ones in flexural toppling, while the toppled blocks are also less than the ones in block toppling. For the above various types of toppling failure, Chigira (1992), Bobet (1999), Wyllie and Mah (2004), Alejano et al. (2010, 2015), Aydan (2016), and Sarfaraz (2020) pointed out different types of toppling failures associated with actual anti-dip slopes. Stead and Wolter (2015) showed the toppling behavior of a steep overhanging anti-dip slope, in which rock layer thickness and the unsupported length may be critical in influencing the toppling process and behavior. Huang et al. (2013) studied the Kuantan landslide due to an Mw 8.0 earthquake in Wenchuan, China. The rock slope is an anti-dip slope with toppling failure. A total volume of 4.68 million m^3 of rock masses slid into the nearby river, resulting in a debris dam. In the upper part of the slope, it was found that interlayer-shearing-induced toppling could lead to a large-scale landslide of the slope subject to an earthquake event. In another case in Taiwan, an anti-dip slope failure occurred close to the riverbank of Putanpunas Stream (Lo 2017). In this case, the defects in the deformed rock layers formed a potential sliding plane, and finally, the rock mass above the sliding plane slid down and caused significant disaster to the downstream areas. In summary, interlayer slip failure could be formed in the rock layers of anti-dip slopes subject to gravitational deformation. Flexural toppling or block toppling could occur under different geological or geometrical properties, such as the angle and the spacings of the weak planes.

Analysis approaches for anti-dip slopes

Goodman and Bray (1976) proposed a simple kinematic condition necessary for the flexural slip before toppling. Assuming that the major principal stress to be oriented in the direction parallel to the dip direction, it has been shown that the necessary condition for the flexural slip to occur is:

$$\alpha \geq 90 + \phi - \beta$$

where α is the slope face dip angle, φ is the interlayer friction angle, and β is the dip angle of the bedding plane or weak planes. Stereonet analysis can also be applied to analyze the possible failure mechanisms with the orientations of the relevant bedding or slope planes.

Cruden (1989) extended the above equation to show that the maximum angle between the slope face and the dip direction of the discontinuity that allows toppling depends on the friction angle of the discontinuities and the slope angle when the discontinuities dip into the slope. Bobet (1999) derived analytical solutions for block toppling under dry and seepage conditions. Amini et al. (2009, 2012) proposed analytical solutions for flexural toppling and block-flexure toppling respectively. Majdi and Amini (2011) studied the geo-structural defects in flexural toppling from fracture mechanics and a case study. Zheng et al. (2019) explored block-flexure toppling using theoretical approaches and numerical (discrete element) models. Gui et al. (2024) explored the toppling behaviors of blocks misaligned with slope faces from analytical and experimental studies.

Adhikary et al. (1997) and Adhikary and Dyskin (2007) applied geotechnical centrifuge tests to study the scale

effect of the block and flexural toppling. Ductile and brittle materials were used to simulate different toppling behavior. Alzo'ubi et al. (2010) also employed centrifuge tests to study the effect of the tensile strength of the interlayer rock columns on the toppling behavior. Nishimura et al. (2012) applied small-scale laboratory tests to investigate the flexural toppling behavior when subject to pulsating horizontal loadings. Amini et al. (2012) also studied the deformation features of anti-dip slopes with different weak plane angles based on site investigation results. Steep weak plane angles commonly lead to toppling failure, while gentler angles can result in shear failure of the rock layers when the toe of the slope is eroded. Nichol et al. (2002) used field investigation and UDEC analysis to investigate the effect of rock mass strength, joint orientation, and joint persistence on the toppling behavior of anti-dip slopes. It was found that the ductile material produced slow and flexural toppling, while brittle material gave fast block toppling. Zheng et al. (2024) investigated the flexural toppling failure of rock slopes using finite discrete element models. Parametric studies by varying the geological parameters of joint angles, slope angles, and thickness of rock layers were also conducted.

Based on the above discussion, it is inferred that the toppling behavior of anti-dip slopes might be related to the geometrical and mechanical properties of the rock slope, such as the tensile strength of the rock mass, joint properties, rock layer thickness, unsupported length of the slope face and the weak plane angle. Furthermore, the scale of the slope itself may also be a critical factor affecting the anti-dip slopes' deformation features. The above discussions also revealed that the toppling behavior associated with anti-dip slopes could be studied with site investigation and physical modeling. The application of centrifuge modeling is essential to understand the scale effect. In this study, we would like to employ the above research approaches to investigate the deformation features of a steep overhanging anti-dip slope considering the geometrical properties, including the rock layer thickness, unsupported length of the slope face and the slope scale, hoping to capture the overhanging anti-dip slope failure patterns that we observed in the field and explore the affecting factors on the toppling behavior of overhanging anti-dip slopes from material mechanics viewpoint.

Study approaches

Site investigation

The site is located in the slate belt of the western Backbone Range (Fisher et al. 2002), close to a riverbank of Tienkooer Creek in Yilan County, Taiwan. It displays a well-exposed cliff with a height of approximately 6.5 m and a width of a few tens of meters (Fig. 1). The cliff mainly consists of slate with dense fissile cleavages. The spacings of the dominant parting surfaces resulting from weathering cleavages are approximately several centimeters to 20 centimeters. There is a 2-meter-wide gully cutting into the cliff, but it is now filled with debris. Due to three Typhoon events in 2009, 2010, and 2012, siltation and scouring events occurred alternatively at the site, likely in particular to the gully. During site investigation, the common deformation feature of flexural toppling was observed that the upper part (deformed) of the rock layers showed a cleavage angle of about 35 to 40 degrees, while the lower part of the rock layers (undeformed) expressed the cleavage angle of around 70 to 75 degrees, as shown in Fig. 1(a). Fractures or tension cracks were also observed in some locations within the rock layers (Fig. 1(b).

Geotechnical centrifuge modeling

The stress levels in physical model tests are critical for obtaining reasonable mechanical responses of the prototype models, such as the deformation behaviors of rock slopes in the field. In this study, we utilized an in-house geotechnical centrifuge facility to conduct physical tests under the specified centrifugal gravity. We aimed to replicate the stress levels of the anti-dip slope in the field. Therefore, during the centrifuge tests, we can apply various gravity fields to the physical models, allowing the model parameters or responses to be adjusted according to the given scaling factors. The stress, strain, and other physical properties between the physical and prototype models can be obtained using the corresponding scaling laws. For instance in Table 1, under a gravity field of n-g, the stress, and strain in both the physical and prototype models are identical, while the length, force, and unit weight differ between them.

The capacity of the NCU (National Central University, Taiwan) geotechnical centrifuge is 100 g-ton, with a nominal radius of 3 m. With the onboard weights of the equipment, the maximum payload is 400 kg under a maximum centrifuge acceleration of 80 g. By rotating the mechanical arm, on which the physical models are placed, at a specified angular velocity (revolutions per minute, rpm), the required gravity field can be achieved in the physical models. Two video recording systems were installed inside the testing box to monitor the deformation of the overhanging anti-dip slope during the centrifuge testing. Each system takes photos and videos from the top and side views. The simplified overhanging anti-dip slopes were placed inside the rigid testing box made of aluminum alloy (inner dimensions of L×W×H are $736 \times 200 \times 370$ in mm), with one side being a transparent acrylic panel to monitor the deformation behaviors laterally.

As discussed previously, we would like to simulate the toppling behavior due to the gravitational effect of the overhanging anti-dip slope. Therefore, the simplified

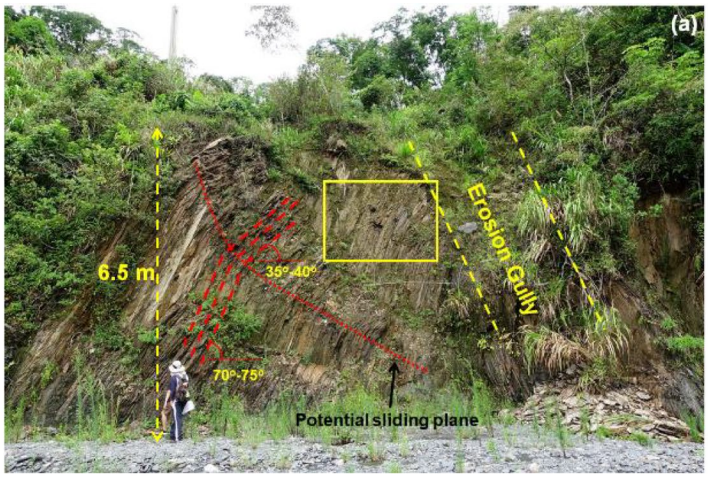

(a) Flexural toppling of an anti-dip slope in Yilan County, Taiwan

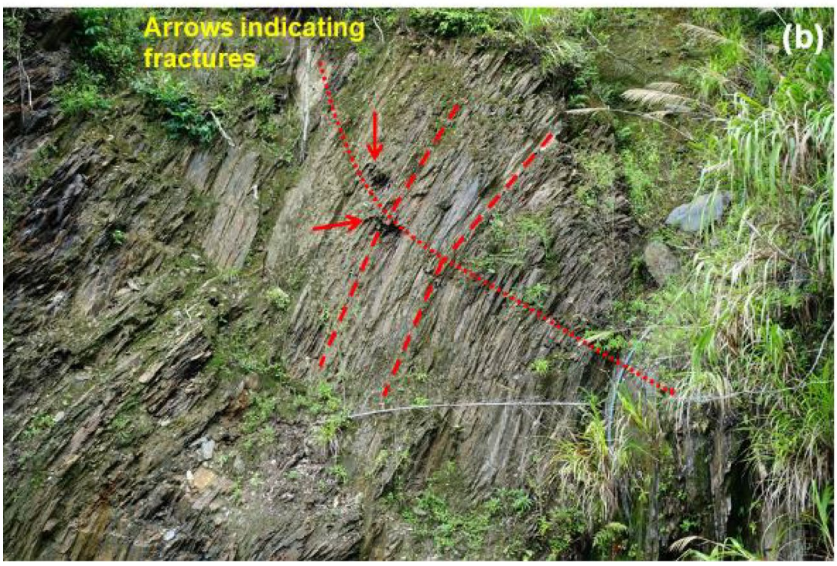

(b) Fractures in the rock layers (zoomed-in view of the box in (a))

Fig. 1 (**a**) Flexural toppling of an anti-dip slope in Yilan County, Taiwan.(**b**) Fractures in the rock layers (zoomed-in view of the box in (a))

Table 1 Scaling law between the physical and prototype models

Parameters	Imperial Units	Scaling Factor (Physical model/Prototype)
Acceleration	m/sec^2	n
Length	m	1/n
Force	Newton (N)	$1/n^2$
Stress	N/m^2	1
Strain	-	1
Unit Weight	N/m^3	n

overhanging anti-dip slope models were created using 16 single rock sheets or 8 double rock sheets. Each rock sheet consists of rock balls that have a uniform diameter of 5 mm, a weight of 0.58 g, and a specific gravity of 2.54. These rock balls are composed of a mixture of kaolinite, albit, and carborundum in a specific ratio. According to results from direct shear and tilt tests, the basic friction angles of the rock balls are approximately 45 degrees and 32 degrees, respectively. A single rock sheet was made by applying 20 ml of glue mixture between the rock balls, giving a tensile strength of around 570 kPa. The mix contains white glue and pastes with a volume ratio of 1:3. The dimension of a single rock sheet is 20 cm by 6 cm (40 balls in length and 12 balls in width), as shown in Fig. 2.

In an earlier study by Huang et al. (2019), dip slope models were constructed by stacking multiple rock sheets based on specific test configurations, such as weak plane angles and rock layer thicknesses. Rock sheets were chosen over gypsum boards or in-situ rock specimens as physical models because, under the applied testing conditions—such as

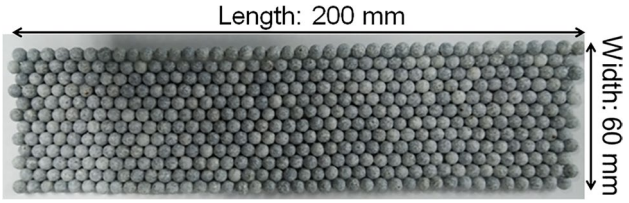

Fig. 2 Dimension of a single rock sheet

increased centrifugal gravity or submersion in water—the strength of these other materials was too high to produce the desired deformation characteristics of dip slopes. However, Huang et al. (2019) observed buckling failure near the toe of the dip slope models, demonstrating that rock sheets made of rock balls can effectively replicate the expected failure patterns of rock slopes. Chen et al. (2020) used gypsum boards to study the seismic responses of anti-dip slope models, with the results indicating that these responses are closely related to the slenderness ratios of the gypsum boards. In contrast, the current study focused on the deformation patterns of overhanging anti-dip slopes. The use of rock sheets, rather than gypsum boards or in-situ rock specimens, may be a viable approach to producing the expected toppling patterns. Additionally, we also assumed an extremely weak condition for the anti-dip slope models, where there is no cohesion between the rock layers, while the other mechanical and dimensional properties were kept consistent with field conditions. For these reasons, we chose to use rock sheets made of rock balls as the fundamental elements to simulate the rock layers in overhanging anti-dip slopes.

Depending on the configuration of the overhanging anti-dip slopes, 16 single rock sheets were placed adjacent to one another to simulate an anti-dip slope composed of thin rock layers. Alternatively, two single rock sheets were bonded face-to-face to create one rock layer. Eight rock layers (each with two rock sheets) were then arranged side by side to simulate an anti-dip slope consisting of thick rock layers. The completed overhanging anti-dip slope model is then placed between the front and back plates and tightened at the bottom part of the rock layers as a fixed-end condition. Once this step was completed, the sand layers were poured into the testing box to the specified height, with an embedment length ranging from approximately 12.5 cm to 8 cm, corresponding to an unsupported length of 7.5 cm to 12 cm, given that the rock sheet length is 20 cm, as shown in Fig. 3(a).

In the testing configurations of the overhanging anti-dip slope models, there are unsupported parts of the rock layers that could deform and even fracture. The unsupported part of the rock layer also simulates the effect of previously-empty erosion gully in the field. As the centrifugal gravity in the slopes increases to the targeted gravity field, the unsupported slope face (overhanging) may deform under the undesired gravity field. For this reason, we have designed a supporting plate activated by a pressurized chamber system placed right in front of the unsupported slope face (Fig. 3). As the centrifuge test initiates, the supporting plate is set against the unsupported part of the overhanging anti-dip slope. Until the targeted gravity is reached, the supporting plate is retracted by releasing the pressurized chamber system remotely from the control room.

Testing plans and definition of deformation features

Based on the field investigation results, the overhanging anti-dip slope deformed and toppled towards an erosion gully that is now filled with debris. With the presence of the previously empty erosion gully, the overhanging anti-dip slope may bend towards the unsupported side of the rock layers and hence result in the deformation of the rock layers. The unsupported length of the overhanging anti-dip slope is about meter-level in the field, and the thickness

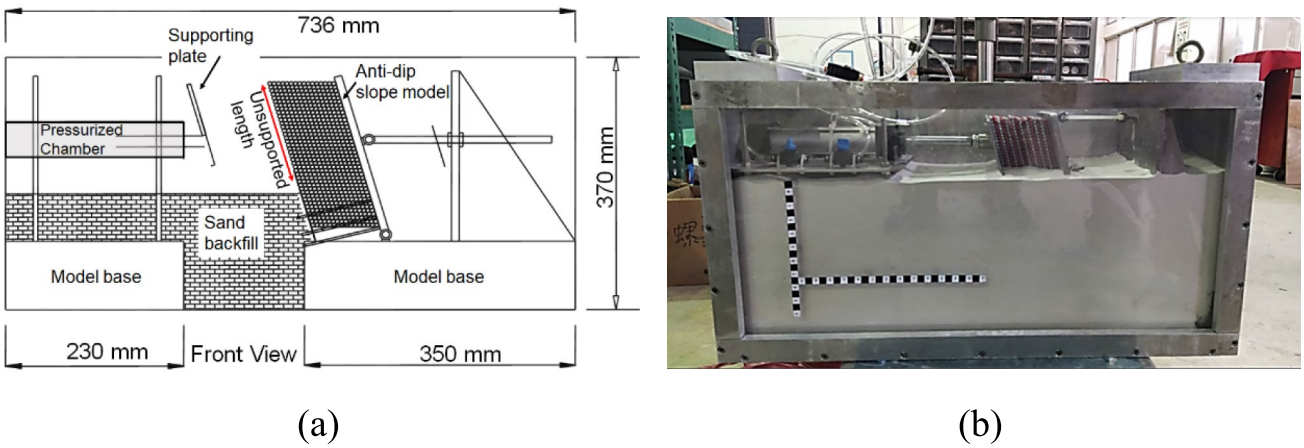

Fig. 3 Overhanging anti-dip slope configuration for centrifuge tests: (**a**) design illustration; (**b**) completed test setup

of the rock layers varies between centimeters to tens of centimeter-level. Moreover, Stead and Wolter (2015) also pointed out that toppling behavior may be related to various parameters, including the geometrical properties of the rock layers. Therefore, in the centrifuge test modeling, the thickness of the rock layer and the length of the unsupported part of the rock layers were selected as the parameters to simulate the deformation of the overhanging anti-dip slopes. Although it is common to observe alternating thick and thin rock layers in anti-dip slopes in the field. In this study, we aim to investigate the effects of rock layer thickness on the deformability of the slopes. Therefore, we configured our physical models with one rock layer thickness at a time to simplify the analysis of the effects of varying rock layer thickness in a single model. Furthermore, the rock layer angle was chosen as 75 degrees, which is close to that of the undeformed rock layers that were observed in the field. The gravity fields applied to the simulated overhanging anti-dip slope are 1-g and 20-g, in order to examine the scale effect and to match a comparable rock layer length in the field. The rock layer thickness in the physical model is 0.5 cm (single rock sheet) and 1 cm (double rock sheets). Based on the applied gravity field, the prototype rock layer thickness is equivalent to 10 and 20 cm. The physical model slope height (unsupported length) was chosen based on the available dimension of the testing box. Finally, the width of the physical model was selected as 6 cm, such that it is wide enough to prevent the potential boundary effects while satisfying the testing box dimension limitation at the same time.

The detailed testing scheme is shown in Table 2; Fig. 4. In the following tests, Tests no. 1 and 2 compare the effect of unsupported rock layer length, Tests 2 and 4, as well as Tests 1 and 3, discuss the effect of rock layer thickness.

To discuss the deformation features of overhanging anti-dip slopes with different configurations, we have defined the following terms to describe various locations in the overhanging anti-dip slope models. The rock layers are numbered from 1 to 16; the larger number indicates a deeper rock layer. For each rock layer, the location where deformation or fracturing occurs is also defined from top to bottom with an increasing percentage relative to the total length of the rock layer. A more detailed illustration is shown in Fig. 5.

Table 2 Testing schemes in the physical models

Test no.	Weak plane angle (degrees)	g-level	Rock layer thickness (cm)	Unsupported length (cm)
Test 1	75	1 g/20 g	0.5	7.5
Test 2			0.5	12
Test 3			1	7.5
Test 4			1	12

Centrifuge test results and discussions

The following sections describe the geotechnical centrifuge test results under a gravity field of 20-g. Without otherwise indicated, all of the dimensions (including the elapsed time) in the text of this section refer to the model dimensions.

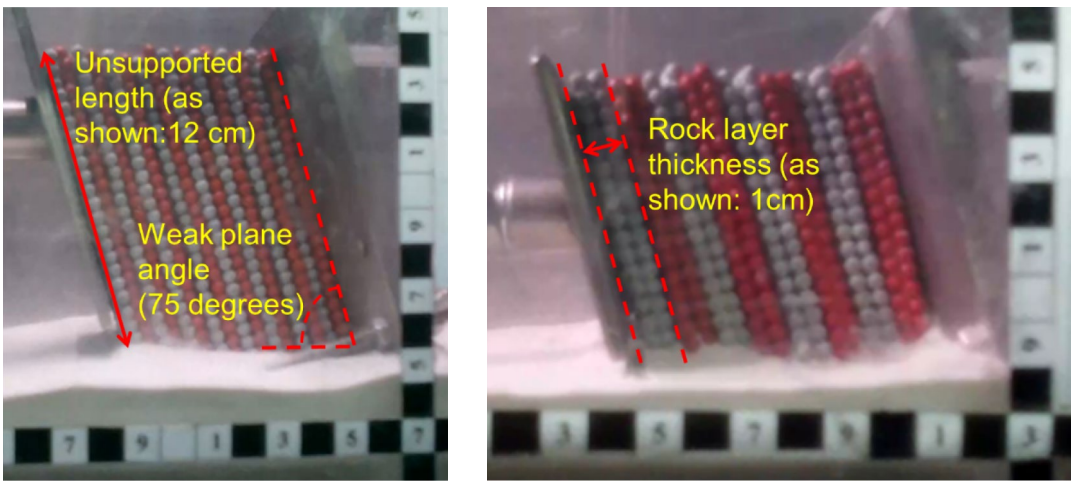

Fig. 4 Definition of (**a**) unsupported length and (**b**) rock layer thickness in the simplified overhanging anti-dip slope models

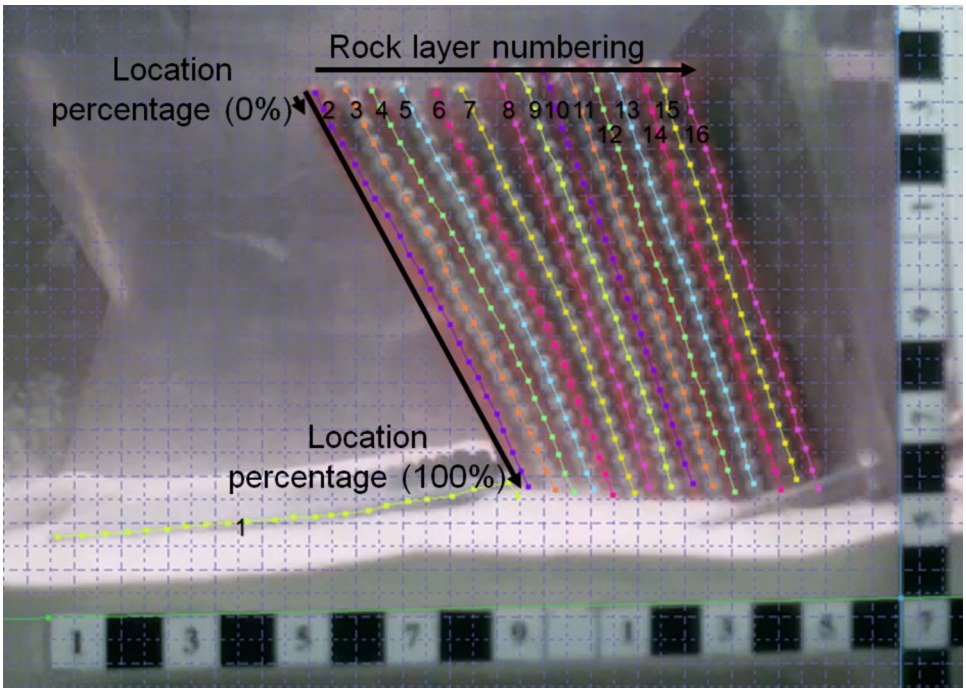

Fig. 5 Rock layer numbering system and deformed/fractured location percentage

Test no. 1 (Rock layer thickness: 0.5 cm, unsupported length: 7.5 cm)

As shown in Fig. 6, the first single rock layer toppled at around 210 s once the supporting plate was released. At about 800 s, the second single rock layer toppled, with the 3rd to 5th rock layers bent forward slightly. With the time increasing, the deformed rock layers toppled up to the 4th rock layer, leaving the 5th rock layer deformed and stabilized. Overall, the stabilized condition was reached at around 825 s. The 6th to the 16th rock layers did not deform at all.

Looking at the locations where the fracture occurred in each rock sheet, the fractured location percentage changed from 100 to 93% to 86% for rock sheets no. 1 to 4. Rock

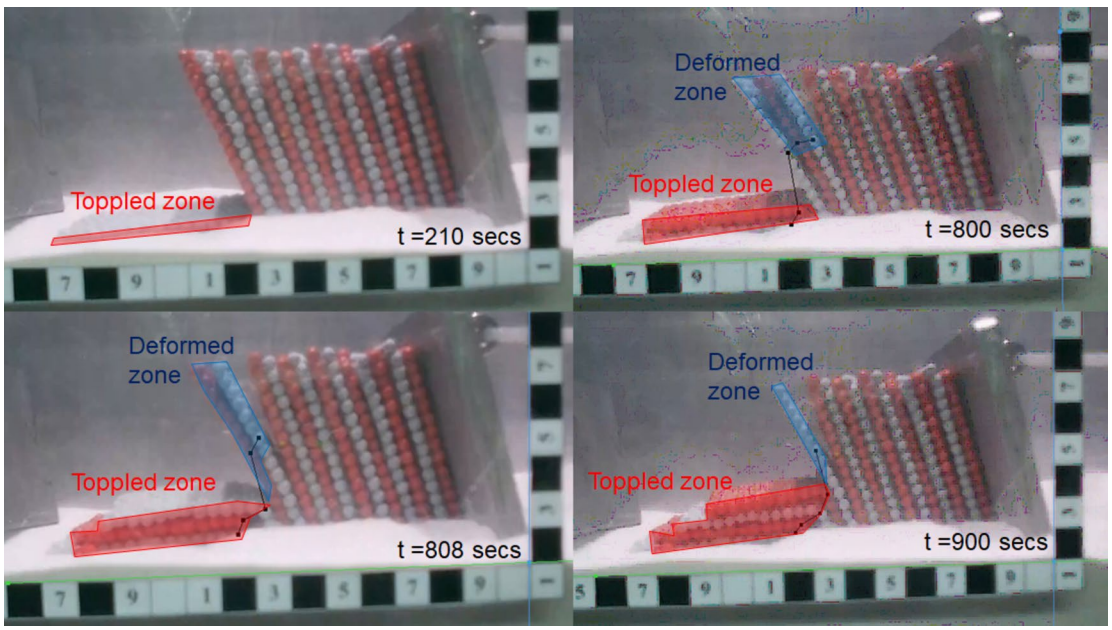

Fig. 6 Test 1: Deformation process and identification of deformed and toppled zones

sheet no. 5 was deformed, and the location was at 50%. An overall summary table is shown in Table 3. It can be inferred that the potential failure (sliding) plane can be developed along the most-fractured places within each rock layer, and the sliding plane propagates upward partially to the slope crest. (i.e., fractured location percentage decreases with the increasing rock layer number.). The deformation behavior in this test is close to block-flexure toppling.

Table 3 Test 1: development of deformation and fractured location percentage with time

Model elapsed time (seconds)	Fractured rock layer no.	Fractured location percentage (%)	Deformed rock layer no.	Deformed location percentage (%)
210	1	100	1	100
800	2	93	3 ~ 5	65
808	3	93	4 ~ 5	80 ~ 57
900	4	79	5	50

Test no. 2 (Rock layer thickness: 0.5 cm, unsupported length: 12 cm)

Figure 7 shows the deformation process of Test no. 2. The 1st rock layer toppled completely at t = 2 s, with rock layers no. 2 to 4 bent forward slightly. Afterward, as time progressed, the shallow, deformed rock sheets fell, and more rock sheets into the rock slope leaned forward. Finally, at t = 985 s, nine rock sheets toppled with two rock sheets bent forward. All of the nine toppled rock sheets stabilized at t = 290 s. Because the unsupported length of rock sheet no. 10 became shorter (i.e., the rock balls of the shallower rock layers accumulated close to the toe), the time for the remaining rock sheets to bend forward became much longer.

The fractured location in each rock sheet was analyzed, and it was found that the fractured location percentage decreases from 96 to 74% to 65% for rock sheets no. 1 to 9, and for rock sheets no. 10 and 11, the deformed location percentage is at about 55%. An overall summary table is shown in Table 4. The deformation feature of this test was very similar to what was observed in the field, i.e., the angles

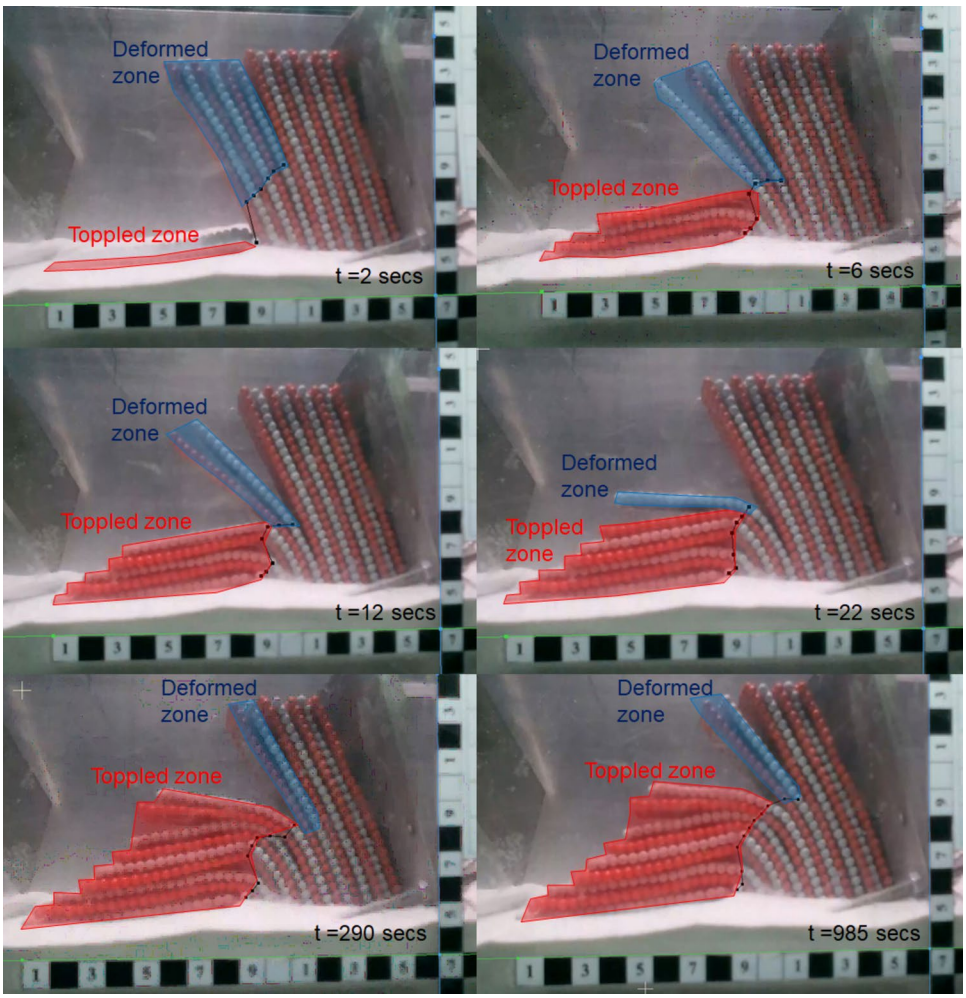

Fig. 7 Test 2: Deformation process and identification of deformed/toppled zones

Table 4 Test 2: development of deformation and fractured location percentage with elapsed time

Model elapsed time (seconds)	Fractured rock layer no.	Fractured location percentage(%)	Deformed rock layer no.	Deformed location percentage(%)
2	1	96	2 ~ 7	74 ~ 55
6	2 ~ 4	74	5 ~ 7	74
12	5	70	6 ~ 7	70
22	6	65	7	57
290	7 ~ 9	65	10 ~ 11	65
985	–	–	10 ~ 11	55

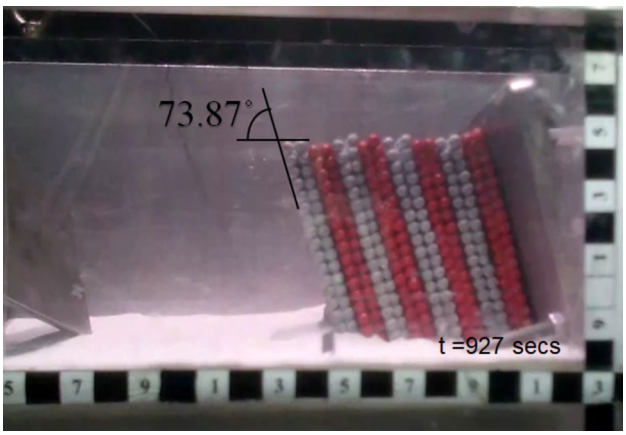

Fig. 8 Test 3: Deformation process and identification of deformed/toppled zones

at the upper and lower parts of the slope were quite different. In addition, based on the test results, a ductile deformation process was also recorded.

Test no. 3 (rock layer thickness: 1 cm, unsupported length: 7.5 cm) and test no. 4 (rock layer thickness: 1 cm, unsupported length: 12 cm)

For Test no. 3, there was no sign of deformation or toppling, as shown in Fig. 8. An even higher gravity field of 40 g was applied to the same model, and still no sign of deformation.

In Test no. 4 (Fig. 9), the first layer (double-rock-sheet) toppled at t = 32 s. Afterward, at a much longer time t = 1192 s, the second and third double-sheet toppled and rested on the debris of the first double-sheet. Finally, the third double-layer entirely rested on the debris of the toppled material at t = 1199 s, with no deformation of the remaining rock layers in the rock slope. The fractured location percentage within each double-sheet varies from 100 to 91%. An overall summary table is shown in Table 5. Compared to the

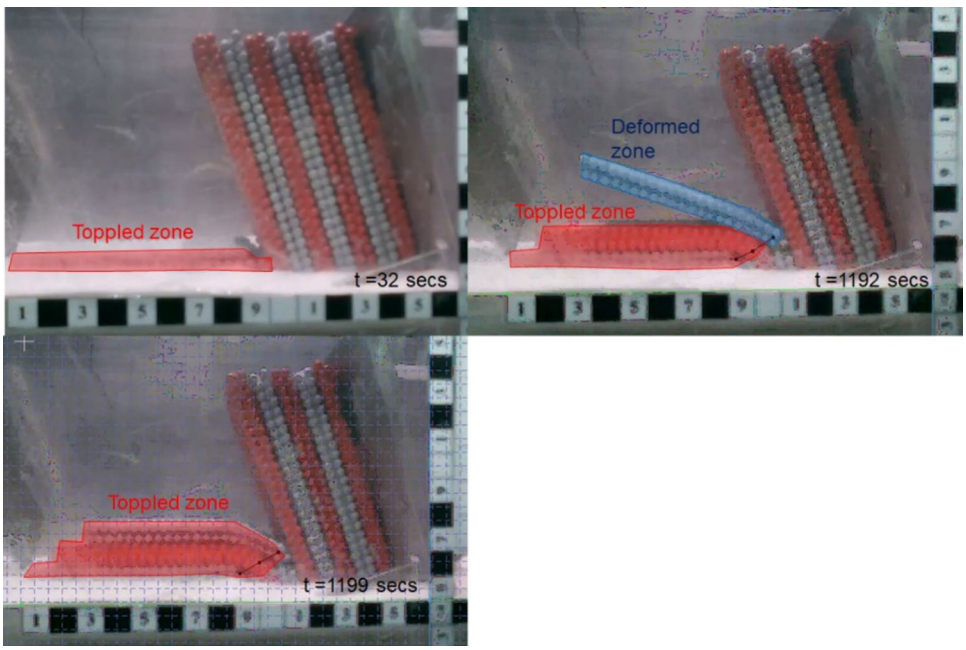

Fig. 9 Test 4: Deformation process and identification of deformed/toppled zones

Table 5 Test 4: development of deformation and fractured location percentage with time

Model elapsed time (seconds)	Fractured rock layer no.	Fractured location percentage(%)	Deformed rock layer no.	Deformed location percentage(%)
32	1 ~ 2	100	–	–
1192	3 ~ 4	96	5 ~ 6	91
1199	5 ~ 6	91	–	–

developed sliding planes in Tests 1 and 2, we can observe a stepwise failure plane for this test. Overall, the deformation process of this test is close to block toppling with brittle behavior.

The effects of slope scale, rock layer thickness, and unsupported length on the toppling behavior

General discussion

The steep overhanging anti-dip slopes with different rock layer thicknesses and unsupported lengths showed standard and various deformation features. First, three tests (Test no. 1, 2, and 4) showed toppling and deformation of the rock layers. The tests showed flexural to block-flexure toppling behavior.

The location where the rock layers are fractured and deformed was discussed in Section 4. For shallow rock sheets in Tests 1, 2, and 4, toppling-induced fracture occurred directly close to the bottom of the rock sheets. For the subsequent rock sheets, the fractured or deformed location moves upward from the bottom, as shown in Fig. 10(a), (b), and (c). Further, if the most-fractured or most-deformed (i.e., maximum curvature) locations within each rock sheet were connected, a potential failure plane could be formed, as shown in Fig. 10(a) and (b). The debris above the potential failure plane could slide above the plane and cause debris accumulation close to the toe of the rock slope. The outcome could be the potential disaster for anti-dip slopes subject to gravitational deformation or other disaster-triggering factors. In Fig. 10(c), the potential failure plane is stepwise, showing that a thicker rock layer may induce a brittle deformation behavior, and hence, block failure could be observed for this test. The following sections discuss the scale effect and the influences of the unsupported length of rock sheets and the rock layer thickness on the deformation features of overhanging anti-dip slopes.

Scale effect on the overhanging anti-dip slope

As mentioned in Table 2, we have performed the overhanging anti-dip slope simulations under gravity fields of 1-g and 20-g. The centrifuge test results have been discussed in the previous sections. For test results under 1-g, Tests no. 1, 3, and 4 yielded no deformation after several days of observation. Therefore, the scale effect is discussed for Test no. 2. As shown in Fig. 11 with Test 2 in 1-g, it can be observed that even after six days of testing, the rock sheets only deformed slightly without any toppling. However, as mentioned previously, as the gravity field increased to 20-g, within less than 1000 s, the rock sheets toppled and deformed significantly. The deformation behavior difference is because the strength of the rock layers is constant, while the increase of gravity field results in the rise of the overturning moment against the toe. The increase in slope size can induce more zones of deformation and toppling. The comparison also indicates that the deformation zone propagates into the slope with the increase in slope size. The time to reach stabilization also shortened with the rise of the slope height.

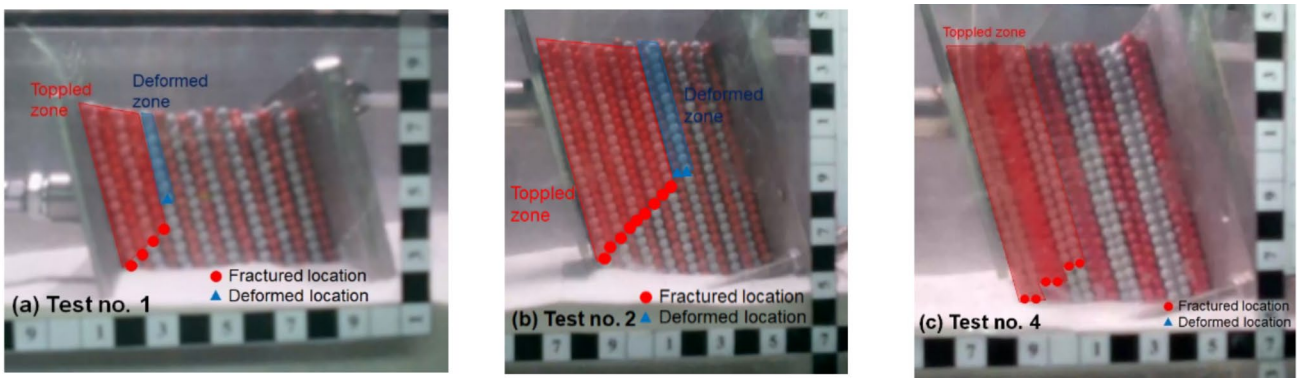

Fig. 10 Fractured and most-deformed locations in the rock layers circled in the un-deformed slope (**a**) Test 1; (**b**) Test 2 and (**c**) Test 4

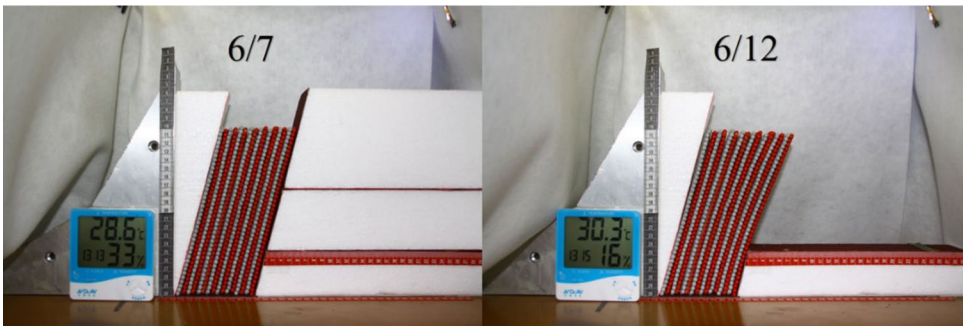

Fig. 11 Test 2 (g-level = 1-g): deformation process (left: day 1, right: day 6)

The effect of unsupported rock layer length

Tests 1 and 2 showed the effect of unsupported length under the gravity field of 20-g. The model (prototype) unsupported lengths are 7.5 cm (150 cm) and 12 cm (240 cm). Figure 12 shows the final stage of the two tests. For Test 1, the first four sheets toppled, with one rock sheet slightly deformed. Most of the toppled rock sheets showed fracturing close to the bottom of each rock sheet. The remaining rock sheets did not deform at all. For Test no. 2, the 1st rock sheet toppled at the bottom of the rock sheet. However, the remaining eight toppled rock sheets showed flexural behavior. When looking at the rock sheets, fracturing can also be spotted at different locations. The slightly deformed rock sheets after the 9th toppled sheets extend more into the rock slope.

The effect of the unsupported length of the rock sheets showed distinct toppling behavior of the anti-dip slopes. First, smaller unsupported lengths may show close-to-rigid (or hard) toppling behavior; fracturing can be found close to and above the toe of the slope. For longer unsupported length, except for the 1st hard toppling rock sheet, the toppled rock sheets deformed first and bent forward until fracturing occurred along the rock sheets. The deformation behavior is close to flexural toppling. Secondly, the percentage of the toppled and deformed zones was calculated using the following definition:

Percentage of toppled (deformed) zones = no. of toppled (deformed) rock balls above the toppled (deformed) location / total rock balls.

With the above definition, Test 1 expressed fractured and deformed zone percentages of 23% and 5%. In comparison, Test 2 showed 41% and 7%, as shown in Fig. 12. The difference may indicate that if the unsupported length is short, the toppling behavior may only extend to a small portion of the whole slope. However, on the other hand, slopes with longer unsupported lengths may deform with flexural toppling and continue to the inner slope with a higher deformation percentage.

The effect of unsupported length between Tests 3 and 4 with double-rock sheets can also be investigated. With a smaller unsupported length in Test 3, only Test 4 showed hard toppling behavior, and the failure extended to a small portion of the whole slope, while Test 3 had no deformation.

The effect of rock layer thickness

Tests 2 and 4 showed the effect of rock layer thickness under the gravity field of 20-g, with Test 2 being discussed in the previous section. Test 4 shows distinct toppling behavior compared to Test 2 with thinner rock layers, as in Fig. 13. All of the toppled double-rock sheets fractured close to the toe of each rock layer, and the remaining rock sheets deformed

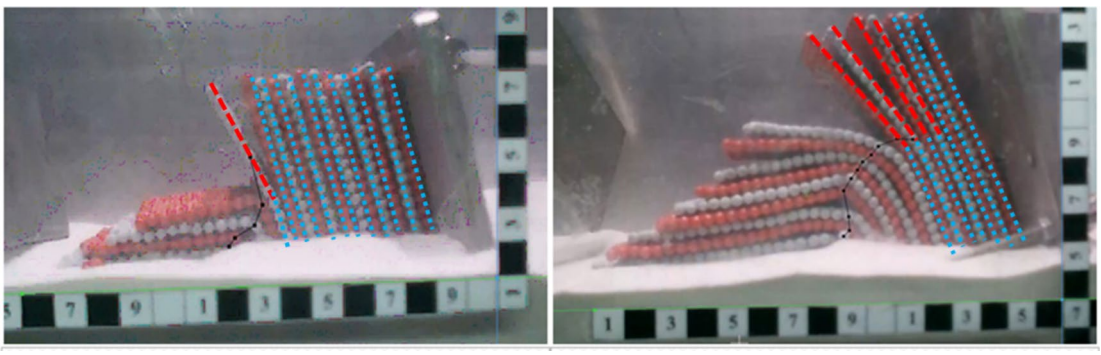

Fig. 12 The effect of unsupported length – left (7.5 cm, Test 1) and right (12 cm, Test 2)

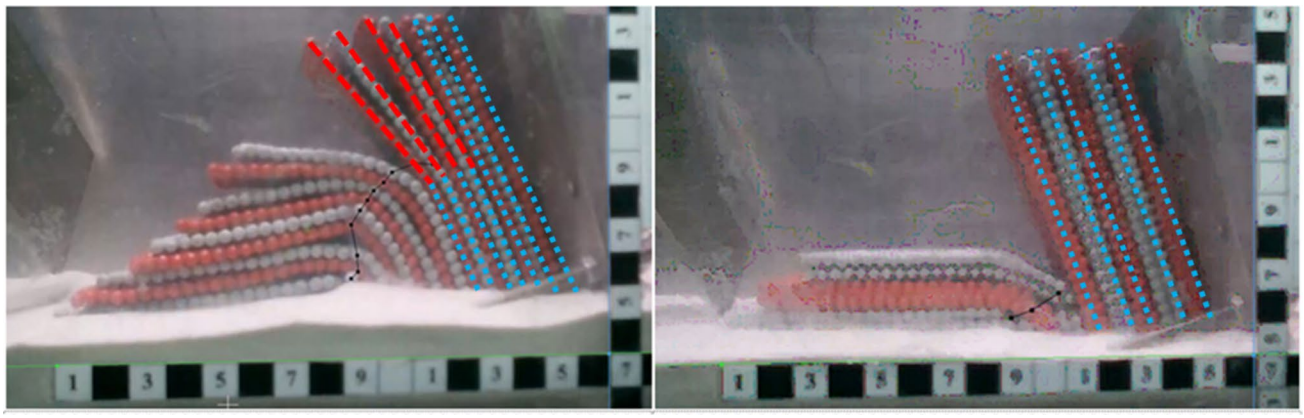

Fig. 13 The effect of rock layer thickness – left (0.5 cm, Test 2) and right (1 cm, Test 4)

insignificantly. (The last double-rock-sheet moved slightly away from the supporting plate). Again, for the same unsupported length, the overhanging anti-dip slope with thicker rock layers showed hard toppling behavior with the fractured location close to each rock sheet's end. However, the thinner rock layer slope exhibited flexural toppling behavior. Finally, the percentage of fractured and deformed zones for Test 4 is 36% and 0%. The percentage is slightly different from Test 2 with thinner rock layers. However, in Test 2, the potential sliding plane is continuous and propagating upward into the slope. In contrast, for Test 4, the sliding plane is stepwise and cannot propagate further into the slope. The above result may infer that the rock layer thickness of the overhanging anti-dip slopes could influence the failure pattern and degree of propagation of the potential sliding plane. Hence, we anticipate that the deformability of the model with alternating rock layer thicknesses is influenced by the location of the "thick" rock layer. In other words, under favorable conditions where the anti-dip slope is prone to deformation, the deformed rock layers may extend deeper into the slope until a relatively thick layer is encountered.

The effect of rock layer thickness can also be explored between Tests 1 and 3 with the same unsupported length. With a thicker rock layer in Test 3, only Test 1 showed hard toppling behavior, and the failure extended to a small portion of the whole slope, while Test 3 had no deformation.

Discussing the deformation behavior from a material mechanics perspective

Based on the above discussion, it can be found that toppling behavior is highly related to the unsupported length, rock layer thickness, and slope size. With the above geometric factors combined, we would like to explore the deformation behavior from a material mechanics perspective. The main idea is to consider a single rock layer as a cantilever beam fixed at the ground surface. As shown in Fig. 14, the

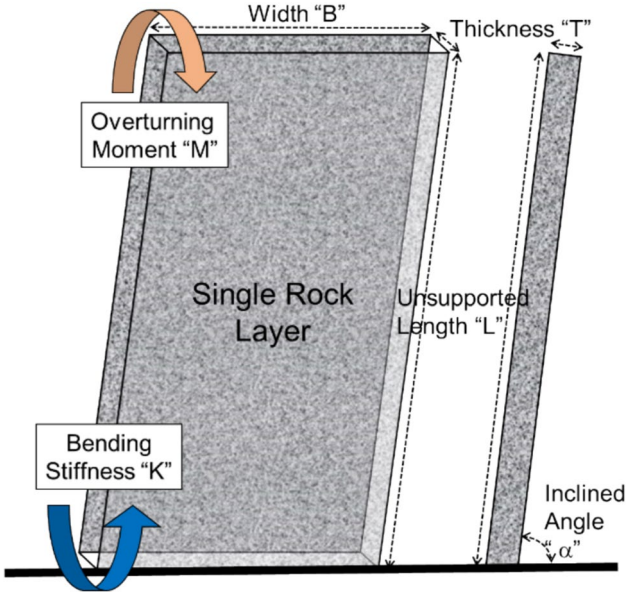

Fig. 14 Geometric definitions of a single rock layer (left: front view; right: side view)

self-weight of a single rock layer would apply an overturning moment to the bottom of the rock layer. Assuming that the thickness of the rock layer is T, the length above the ground surface (unsupported length) is L, the width is B, the inclined angle is α, its unit weight is γ and the Young's Modulus is E. The overturning moment against the bottom of the single rock layer can be expressed as M:

$$M = \gamma BLT\left(\frac{L}{2}\right)\cos\ \alpha$$

On the other hand, the bending stiffness (K) can be calculated as the flexural rigidity (EI) of the member divided by the length (L) of the member. The bending stiffness can be regarded as the required moment to induce a unit rotation

angle; therefore, it can be treated as the resistance against bending. Based on the definition, the bending stiffness K can be calculated as:

$$K = \frac{EI}{L} = \frac{E\left(\frac{1}{12}BT^3\right)}{L}$$

M and K in the above equations represent the induced moment in the single rock layer and the ability (moment) to resist bending. Therefore, we define the dimensionless term "the Normalized Bending Stiffness" K' (K prime) to represent the ability of the single rock layer to bend forward. Specifically, the following K' is derived under 1-g gravity field condition.

$$K'_{(1-g)} = \frac{K}{M} = \frac{\frac{E\left(\frac{1}{12}BT^3\right)}{L}}{\gamma BLT\left(\frac{L}{2}\right)\cos\ \alpha} = \frac{ET^2}{6(\rho g)L^3\ \cos\ \alpha}$$

The above equation of the normalized bending stiffness K' indicates that the length, thickness, and the inclined angle of the rock layer could influence the normalized bending stiffness. As the Young's modulus (E) and thickness (T) are larger, the K' value is also larger, indicating that the rock layer is more difficult to bend forward due to self-weight. On the other hand, as the unit weight (γ), length (L), and cosine (α) are larger, the K' value is smaller, making the rock layer more prone to bend forward.

The normalized bending stiffness K' needs to be re-evaluated in the centrifugal environment. Assuming that the applied gravity field is n-g, then the model K' can be expressed as:

$$K'_{(model\ type:n-g)} = \frac{K}{M} = \frac{\frac{E\left(\frac{1}{12}BT^3\right)}{L}}{\gamma BLT\left(\frac{L}{2}\right)\cos\ \alpha} = \frac{ET^2}{6(png)L^3\cos\ \alpha} = \frac{K'_{(model\ type:1-g)}}{n}$$

Finally, because the normalized bending stiffness is dimensionless, the scaling law of the K' between the model and prototype conditions is 1. Hence:

$$K'_{(proto\ type:n-g)} = K'_{(model\ type:n-g)} = \frac{K'_{(model\ type:1-g)}}{n}$$

In the following discussions, the K' values were estimated based on the individual experimental settings and the Young's Modulus of the rock ball is 3 GPa with the unit weight of 25.5 kN/m^3 (Lo et al. 2014). All other geometric parameters can be found in Table 2.

Table 6 shows the normalized bending stiffness for all tests under 1-g and 20-g gravity fields. Based on previous discussions of lab test results, it can be found that Test 2 under 1-g showed negligible deformation of the rock layers after five days of testing. Tests 1, 3, and 4 under 1-g showed no deformation. Looking at the normalized bending stiffness K' under 1-g in Table 6, it can be found that Test 2 has the smallest K' among all tests under 1-g. However, this value is still larger than Tests 1 to 4 under 20-g gravity field. It is inferred that the normalized bending stiffness is negatively correlated to the degree of the toppling of the rock layer. As discussed for test results under 20-g, only Test 3 showed no sign of displacement, while Tests 1, 2, and 4 showed various degrees of toppling behavior. If the toppling behavior is expressed as the toppling and deformed zone% as calculated earlier, Fig. 15 shows that the smaller the K' value, the larger the toppled and deformed areas. A smaller K' value may indicate a larger deformation zone, which could be toppled later. On the other hand, Fig. 15 also inferred that the toppling behavior can occur with a threshold K' value less than 28. Although there are no other tests with in-between K' values to pinpoint the threshold value, this range could be employed to roughly estimate if the toppling could occur under the testing conditions applied in this study. Please also note that the fracturing of the rock layer needs to be evaluated based on its strength parameters, such as the tensile strength of the rock layer. The normalized bending stiffness is used here to evaluate the ability of the rock layers to deform.

Furthermore, considering the time to reach stabilization of each test, Test 4, 1, and 2 took 1192, 825, and 290 seconds, while Test 3 yielded no deformation. We found that the time for stabilization is also highly related to K', as shown in Fig. 16. With the low K' (as low as 6.8), the toppling could occur relatively quickly.

During the site investigation, we also measured the thickness (0.20m), the unsupported length (6.7m), and the dip angle(75^o) of the rock layers. Based on a local engineering report about the repair of the Tienkooer Bridge in 2013,

Table 6 Normalized bending stiffness (K') of centrifuge tests

Test no.	EI/L (1 g) Bending Stiffness (K) (kN-m)	M (1 g) Overturning Moment (kN-m)	$K'_{(1\ g)}$ Normalized Bending Stiffness (1 g)	$K'_{(20\ g)}$ Normalized Bending Stiffness (20 g)
Test 1	0.0104167	0.0000186	561.177	28.059
Test 2	0.0065104	0.0000475	137.006	6.850
Test 3	0.0833333	0.0000371	2244.708	112.235
Test 4	0.0520833	0.0000950	548.024	27.401

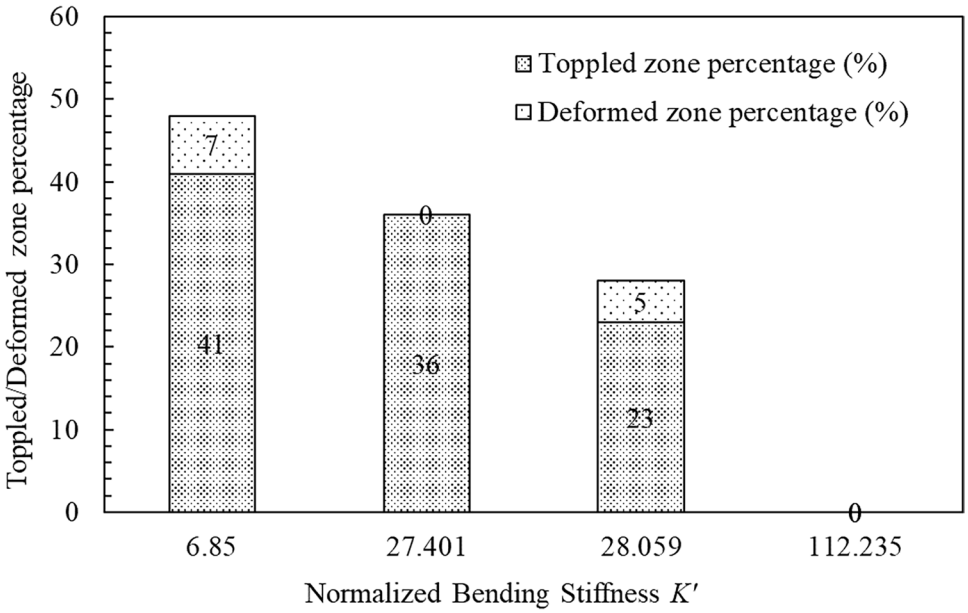

Fig. 15 The histogram of toppled/deformed area percentage and K' values

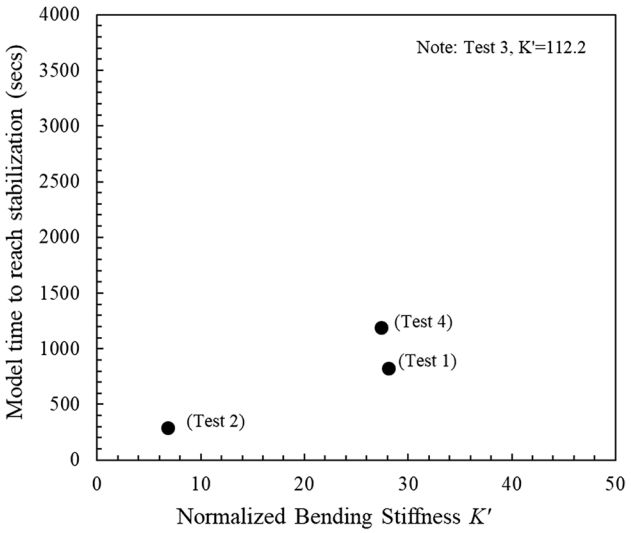

Fig. 16 The relationship between time for stabilization and K' values

the elastic moduli ranged from 0.2 to 3.6 GPa, which were determined through uniaxial tests of the in-situ slate layers. The unit weights of typical rock specimens or rock balls in this study were also quite consistent. Therefore, for simplicity in simulation and analysis, we assumed that the elastic moduli and unit weights of the in-situ slate specimens and rock sheets are 3GPa and 25.5 kN/m^3, respectively. The normalized bending stiffness at the site (K') was estimated as:

$$K'_{(field\ investigation)} = \frac{K}{M} = \frac{\frac{E\left(\frac{1}{12}BT^3\right)}{L}}{\gamma BLT\left(\frac{L}{2}\right)\cos\ \alpha} = \frac{1492(kN-m)}{1185(kN-m)} \approx 1.26$$

The K' of the site (1.26) shows that it is much smaller than the lower bound threshold value of 28 (Tests 1 and 4 under 20-g), which means that the rock layers in-situ are highly prone to flexural toppling. Furthermore, the in-situ K' value is approximately the K' value of Test 2 under a 100 g gravity field (K'=6.8/5 = 1.37). Under this gravity field, the rock layers could bend forward easily, and possibly, due to the insufficient tensile strength of the rock layers, the rock layers of the overhanging anti-dip slope in the field expressed fractures, especially at the locations in the rock layers where the maximum curvature exist. Although the calculation of in-situ K' did not consider the cohesion between the in-situ rock layers at present, the existing flexural toppling at the site may suggest that there was a significant strength deterioration between the rock layers in the distant past. It should be noted that toppling behavior is related to the mechanical, geological, and geometric properties of the rock layers in the overhanging anti-dip slope. In the current study, only the geometric properties (length and thickness of the rock layers) were analyzed from a material mechanics viewpoint.

Overall, the test results showed flexural and block toppling behavior. The flexural toppled rock layers bend forward initially, and with the increase of time, the rock layers lay down on the ground surface, with fractures occurring close to the toe of shallow rock sheets. As time elapsed, more rock sheets into the slope bent forward and deformed. The whole flexural toppling could occur within a relatively short time (as compared to block toppling with the same material). For block toppling, the shallow rock sheets toppled directly, with the fracture occurring close to the bottom of the rock sheet. The rock sheets behind the toppled ones deformed slightly. It can be anticipated that blocks of debris

could be formed with the increase of time and generation of tension cracks normal to the rock sheet along the most-deformed location.

As mentioned previously, the most deformed location within each rock sheet moves upward; hence, a potential failure plane can be formed, as shown in Fig. 10. The debris of the deformed rock sheets could slide down or accumulate. Once the debris was weathered and carried away, the anti-dip slope we usually discover in the field could be formed with the slope face and weak plane planes dipping in opposite directions. Please note that in the simplified overhanging anti-dip slope simulated in this study, each rock layer is intact without any joint perpendicular to the weak planes between rock layers and there is no cohesion between any two adjacent rock layers to simulate extremely weak conditions between the layers. Therefore, the toppling behavior could differ under various geological conditions not discussed in this study.

Conclusions

The deformation features of steep overhanging anti-dip slopes are explored from multiple perspectives, including their scale, the effect of rock layer thickness, and the unsupported length of the slope. Centrifuge tests were performed for multiple configurations of simplified overhanging anti-dip slopes under a g-level of 20-g. The simplified overhanging anti-dip slopes consisted of rock sheets made of rock balls 5 mm in diameter.

For all the centrifuge tests performed in this study, the steep overhanging anti-dip slopes expressed flexural and block toppling behavior. Fractures developed in the rock layers, and the fracture locations tended to become shallower as the layers deepened within the slope. The fractured spot (potential tension cracks) in each rock layer could form a potential sliding plane. Flexural toppling progressed gradually: initially, the shallower rock layers deformed slightly, then they toppled, causing the underlying layers to deform in turn.

Four tests were performed under centrifugal and regular gravity fields. Among the four test configurations, only Test no. 2 (rock layer thickness of 0.5 cm and unsupported length of 12 cm) showed deformation under both 20-g and 1-g gravitational fields. However, under 1-g, it took approximately six days for Test No. 2 to exhibit minimal deformation. When Test no. 2 is under 20-g, the shallow rock layers toppled (rock layers no. 1 to 9), and deep rock layers (no. 10 and 11) deformed slightly. This suggests that increasing the scale of the slope leads to a wider toppled and deformed zone in the overhanging anti-dip slope.

As the unsupported length of the slope face is long, the deformation behavior tends to be dominated by flexural toppling. In such cases, a larger portion of the slope becomes deformed, and stabilization is reached more quickly. As the rock layer thickness increases, the deformation behavior shifts toward block-flexure toppling. In this study, a dimensionless term "normalized bending stiffness" (K') was proposed to evaluate the ability of the rock layers to bend. From a material mechanics perspective, the normalized bending stiffness reflects the balance between the overturning moment due to self-weight and the bending stiffness. The K' values were also derived for the model and prototype under centrifugal conditions. Based on the laboratory test results, it was found that K' is highly related to the toppling behaviors of each test in this study.

For Test No. 2 under both 1-g and 20-g, distinct toppling behaviors were observed, which correlate with the differences in the K' values. The results indicated that K' is closely related to the toppling behavior observed in the tests, confirming that the scale effect influences the deformation characteristics of the rock slope.

By examining the K' of the four tests under 20-g, Test no. 2 (with the smallest value) exhibited the most severe toppled and deformed conditions of the slopes. Despite having different configurations, Tests No. 1 (rock layer thickness of 0.5 cm and unsupported length of 7.5 cm) and No. 4 (rock layer thickness of 1 cm and unsupported length of 12 cm) showed larger K' values, which resulted in a smaller percentage of the slope being deformed. Test No. 3, with a specific K' value, showed no deformation. Based on the above results, a threshold K' value for the rock layer to bend forward is estimated to be around 28. Similarly, the K' value is positively related to the time for the overhanging anti-dip slope to reach stabilization. The normalized bending stiffness K' was also analyzed using site investigation data, revealing that it closely matches the K' value for Test No. 2 under a 100-g gravity field. A lower K' value suggests more severe flexural toppling behavior, with an increased potential of fractures developing in the rock layers.

Acknowledgements The authors would like to thank the National Science and Technology Council (formerly the Ministry of Science and Technology) of Taiwan for financially supporting this research under contract MOST 108-2625-M-008-009 -.

Data Availability Relevant data of this research may be available to the readers of the journal upon request.

Declarations

Competing interests The authors declare that they have no competing interests.

References

Adhikary DP, Dyskin AV (2007) Modelling of progressive and instantaneous failures of Foliated Rock slopes. Rock Mech Rock Eng 40(4):349–362

Adhikary DP, Dyskin AV, Jewell RJ, Stewart DP (1997) A study of the mechanism of flexural toppling failure of rock slopes. Rock Mech Rock Eng 30(2):75–93

Alejano LR, Carranza-Torre C, Giani GP, Arzúa J (2015) Study of the stability against toppling of rock blocks with rounded edges based on analytical and experimental approaches. Eng Geol 195:172–184

Alejano LR, Gómez-Márquez I, Martínez-Alegría R (2010) Analysis of a complex toppling-circular slope failure. Eng Geol 114(1):93–104

Alzo'ubi AK, Martin CD, Cruden DM (2010) Influence of tensile strength on toppling failure in centrifuge tests. Int J Rock Mech Min Sci 47(6):974–982

Amini M, Majdi A, Aydan Ö (2009) Stability analysis and the stabilisation of flexural toppling failure. Rock Mech Rock Eng 42(5):751–782

Amini M, Majdi A, Veshadi MA (2012) Stability analysis of rock slopes against block-flexure toppling failure. Rock Mech Rock Eng 45:519–532

Ashby J (1971) Sliding and toppling modes of failure in models and jointed rock slopes. Master of Science Thesis, Imperial College, University of London

Aydan Ö (2016) Large rock slope failures Induced by recent earthquakes. Rock Mech Rock Eng 49(6):2503–2524

Bobet A (1999) Analytical solutions for toppling failure. Int J Rock Mech Min Sci 36(7):971–980

Chen CC, Li HH, Chiu YC, Tsai YK (2020) Dynamic response of a physical anti-dip rock slope model revealed by shaking table tests. Eng Geol 277:105772. https://doi.org/10.1016/j.enggeo.2020.105772

Chigira M (1992) Long-term gravitational deformation of rocks by mass rock creep. Eng Geol 32(3):157–184

Cruden DM (1989) Limits to common toppling. Can Geotech J 26(4):737–742

Cundall P (1971) A Computer Model for Simulating Progressive Large Scale Movements in Blocky Rock Systems. Proceedings of the Symposium of the International Society for Rock Mechanics, Society for Rock Mechanics (ISRM), France, II–8

Deng Q, Fu M, Ren X, Liu F, Tang H (2017) Precedent long-term gravitational deformation of large scale landslides in the Three gorges reservoir area, China. Eng Geol 221:170–183

Fisher DM, Lu CY, Chu HT (2002) Taiwan slate belt: insights into the ductile interior of an arc-continent collision. Geol Soc Am 358:93–106

Goodman RE (1989) Introduction to Rock Mechanics, 2nd edn. John Wiley & Sons Ltd., New York

Goodman RE, Bray JW (1976) Toppling of rock slopes. Proceedings of the Specialty Conference on Rock Engineering for Foundations and Slopes 2:201–234

Gui JY, Alejano LR, Cano M (2024) Analytical and experimental studies on toppling behavior of blocks misaligned with the slope face. Bulletin of Engineering Geology and the Environment 83

Huang R, Zhao J, Ju N, Li G, Lee ML, Li Y (2013) Analysis of an anti-dip landslide triggered by the 2008 Wenchuan earthquake in China. Nat Hazards 68(2):1021–1039

Huang WC, Li KC, Hsieh JY, Weng MC, Hung WY (2019) Deformation behaviors of dip slopes considering the scale effect and their geological properties. Bull Eng Geol Environ 79:1605–1617

Lin CH, Hung C, Weng MC, Lin ML, Uzuoka R (2019) Failure mechanism of a mudstone slope embedded with steep anti-dip layered sandstones: case of the 2016 Yanchao catastrophic landslide in Taiwan. Landslides 16:2233–2245

Lo CM (2017) Evolution of deep-seated landslide at Putanpunas stream, Taiwan. Geomatics Nat Hazards Risk 8(2):1204–1224

Lo CM, Weng MC, Lin YH, Liu PJ (2014) Deformation characteristics of consequent slate slopes through a physical model test. J Chin Soil Water Conserv 45(3):165–173

Majdi A, Amini M (2011) Analysis of geo-structural defects in flexural toppling failure. Int J Rock Mech Min Sci 48(2):175–186

Müller L (1968) New considerations on the Vajont Slide. Rock Mech Eng Geol 6:1–91

Nichol SL, Hungr O, Evans SG (2002) Large-scale brittle and ductile toppling of rock slopes. Can Geotech J 39(4):773–788

Nishimura T, Nakamura K, Hiramatsu H, Ueda H (2012) A Study on Toppling Failure of Rock Slopes using Small Scale Laboratory Test. ISRM Regional Symposium – 7th Asian Rock Mechanics Symposium. Seoul, Korea

Sarfaraz H (2020) Stability analysis of flexural toppling failure using the Sarma's Method. Geotech Geol Eng 38:3667–3682

Stead D, Wolter A (2015) A critical review of rock slope failure mechanisms: the importance of structural geology. J Struct Geol 74:1–23

Tang CL, Hu JC, Lin ML, Yuan RM, Cheng CC (2013) The mechanism of the 1941 Tsaoling landslide, Taiwan: insight from a 2D discrete element simulation. Environ Earth Sci 70(3):1005–1019

Weng MC, Lo CM, Wu CH, Chuang TF (2015) Gravitational deformation mechanisms of slate slopes revealed by model tests and discrete element analysis. Eng Geol 189:116–132

Wyllie D, Mah C (2004) Rock Slope Engineering: Fourth Edition (4th ed.). CRC Press. https://doi.org/10.1201/9781315274980

Zheng Y, Chen C, Liu T, Zhang H, Sun C (2019) Theoretical and numerical study on the block-flexure toppling failure of rock slopes. Eng Geol 263:105309. https://doi.org/10.1016/j.enggeo.2019.105309

Zheng Y, Wu R, Yan C (2024) Numerical study on flexural toppling failure of rock slopes using the finite discrete element method. Bulletin of Engineering Geology and the Environment 83